Geomechanics and Engineering, *Vol. 21, No. 4 (2020) 357-369*
DOI: https://doi.org/10.12989/gae.2020.21.4.357

Diffusion-hydraulic properties of grouting geological rough fractures with power-law slurry

Wenqiang Mu[1,2], Lianchong Li *[1,2], Xige Liu[1,2], Liaoyuan Zhang[3], Zilin Zhang[3], Bo Huang[3] and Yong Chen[3]

[1]*Key Laboratory of Ministry Education on Safe Mining of Deep Metal Mines, Northeastern University, Shenyang 110819, China*
[2]*National-local Joint Engineering Research Center of High-efficient Exploitation Technology for Refractory Iron Ore Resources, Northeastern University, Shenyang 110819, China*
[3]*Shengli Oilfield Branch Company, SINOPEC, Dongying 257000, China*

(Received July 22, 2019, Revised March 29, 2020, Accepted April 3, 2020)

Abstract. Different from the conventional planar fracture and simplified Newton model, for power-law slurries with a lower water-cement ratio commonly used in grouting engineering, flow model in geological rough fractures is built based on ten standard profiles from Barton (1977) in this study. The numerical algorithm is validated by experimental results. The flow mechanism, grout superiority, and water plugging of pseudo plastic slurry are revealed. The representations of hydraulic grouting properties for JRCs are obtained. The results show that effective plugging is based on the mechanical mechanisms of the fluctuant structural surface and higher viscosity at the middle of the fissure. The formulas of grouting parameters are always variable with the roughness and shear movement, which play a key role in grouting. The roughness can only be neglected after reaching a threshold. Grouting pressure increases with increasing roughness and has variable responses for different apertures within standard profiles. The whole process can be divided into three stationary zones and three transition zones, and there is a mutation region (10 < JRCs < 14) in smaller geological fractures. The fitting equations of different JRCs are obtained of power-law models satisfying the condition of -2 < coefficient < 0. The effects of small apertures and moderate to larger roughness (JRCs > 10.8) on the permeability of surfaces cannot be underestimated. The determination of grouting parameters depends on the slurry groutability in terms of its weakest link with discontinuous streamlines. For grouting water plugging, the water-cement ratio, grouting pressure and grouting additives should be determined by combining the flow conditions and the apparent widths of the main fracture and rough surface. This study provides a calculation method of grouting parameters for variable cement-based slurries. And the findings can help for better understanding of fluid flow and diffusion in geological fractures.

Keywords: geological fracture; JRC; shear displacement; grout; water plugging

1. Introduction

Grouting technology has been widely used in geotechnical construction projects, such as water plugging in mining, seepage control in traffic engineering, and oil recovery (He *et al*. 2012, Qian *et al*. 2018, Butron *et al*. 2010, Zhao and Zhou 2016, Shi *et al*. 2018). The stability of rock mass is seriously affected by the joints and fissures, and geological fractures provide paths for the flow and transport of water, and mud in rock mass (Dejam *et al*. 2016). Oil recovery from fractured reservoirs is more dependent on natural geological fractures, artificial fractures, and the strong Power-law characteristics of oil flow (Dejam *et al*. 2018). Grouting can block flow paths and change rock properties (Yin *et al*. 2018, Chang *et al*. 2018; Zuo *et al*. 2019). Grouting theory under complex geological conditions has been investigated and optimized to a certain degree, especially for grouting engineering with high sealing requirements. In addition, the mechanism should be deeply studied to analyze the grouting process and guide project construction, considering the requirements of resource conservation, traffic development, and preventing environmental deterioration. The influence of fracture roughness and tortuosity on the prediction of grout flow should also be investigated. Additionally, attention should be paid to the rheological properties of cement grout, the influence of fracture roughness and tortuosity, and the corresponding influence on the characteristics of grout flow (Xiao *et al*. 2017, Dejam 2018, 2019).

The grouting mechanism is closely related to the slurry rheological properties and geometric and mechanical conditions of fractured rock (Gothall and Stille 2009, El Tani 2012, Stromsvik *et al*. 2018). In the current literature, the diffusion radius, grouting pressure, and flow rate are estimated according to the assumption of smooth plane fracture (Sui *et al*. 2015), but the grouting effect is often unsatisfactory, such as slurry leakage from boreholes and improper plugging. The main reason is that the geological fractures in practical engineering are not smooth, but rough surfaces with certain undulations and protrusions and are also accompanied by shear movement and failure. In 1977, the standard roughness profiles for rock mass were proposed by Barton and Choubey (1977), and rough structural planes have been found to be closely related to rock strength (Liu *et al*. 2017). Fracture roughness also

∗Corresponding author, Ph.D., Professor
E-mail: li_lianchong@163.com

http://www.techno-press.org/?journal=gae&subpage=7
ISSN: 2005-307X (Print), 2092-6219 (Online)

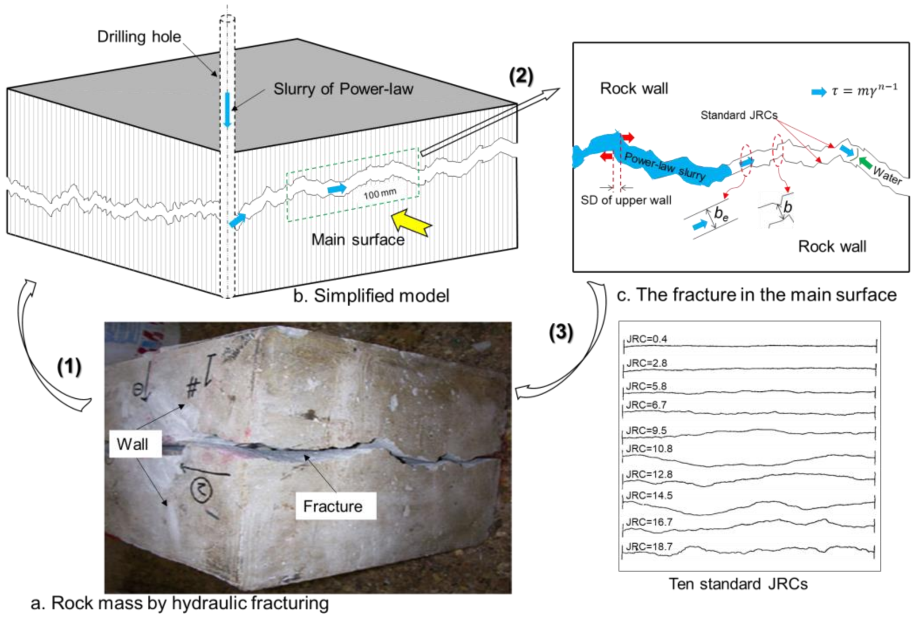

Fig. 1 Sketch of an engineering problem where the fracture roughness and hydraulic properties changed the slurry flow and diffusion

plays an important role in water seepage, water inrush disaster, and variable hydraulic properties (Koyama *et al*. 2008, Sharma *et al*. 2017, Huang *et al*. 2019). With the development of computer simulation software, the mechanism of fluid flow in rough fractures formed by rock mass structural planes has been deeply studied by means of other scanning techniques (Xie *et al*. 2015, Liu *et al*. 2017, Wanniarachchi *et al*. 2018). The undulating trend of rock mass fractures has a greater impact on fluid flow. For grouting slurry, the flow and diffusion are also affected by the fracture walls, which affect the prediction of grouting parameters (Mu *et al*. 2019). There are few studies on grout diffusion characteristics under the characterization of standard geological fracture roughness.

In addition, considering the influence of slurry flow characteristics, some complex rheological models have been developed from a single property. The time-varying characteristics of a Newtonian body and the formula for calculating the maximum diffusion radius of grouting have been discussed (Zhang *et al*. 2017, Funehag and Gustafson 2008). Other types of grouting such as Bingham fluid have also been carried out by the grouting mechanism. Cement grouting exhibits Bingham fluid characteristics for cement-based slurries with a water-cement ratio (W/C) from 0.7 to 1.0, and the flow-core effects can be predicted in the grouting flow and diffusion (Amadei and Savage 2001). However, in many cases, high water-cement ratio slurries cannot have a good effect on water plugging Cui (2011). The higher viscosity makes the grout of W/C 0.5 difficult to diffuse in a rock facture. However, the slurry is often used instead of the original slurry. Therefore, the flow mechanism of low water-cement ratio slurry (power law fluid) should be further studied and revealed in geological fractures.

However, some rheological behavior and diffusion properties of variable viscosity slurry, such as streamlines, velocity, and viscosity in cross sections, cannot be captured directly from experimental measurements. Numerical simulations can be conducted and are used in many studies for channels or fractures, and the studies faced no major difficulties in simulating the flow (Niya and Selvadurai 2019, Sharma *et al*. 2017, Xie *et al*. 2015, Ozsun *et al*. 2013). Fig. 1 illustrates a simple schematic of the slurry flow via a rough fracture between two upper and lower matrix blocks. The numerical simulation results of the slurry diffusion and flow in the field can be divided into three parts, as shown in Fig. 1.

(1) Based on the fractured rock mass in the tunnel, the grouting can be simplified to a 3D fracture model.

(2) Considering the monitoring difficulty of the 3D roughness distribution in field construction, the main fracture can be simplified to a 2D digital model to determine the geometric parameters and aperture.

(3) Digitized fractures are introduced into the simulation platform, the model can be established and calculated, and grouting parameters in construction site can be revised by using the calculated grout flow diffusion mechanism. Otherwise, the standard roughness of the rock fracture should be prefabricated in advance, and the hydraulic characteristics and parameter distribution of grout can be obtained. After comparison with the standard, the grouting engineering construction can be corrected.

Recently, some studies on fluid flow have been simulated by computational software based on a single fracture (Javadi *et al*. 2010, Niya and Selvadurai 2017, 2019). However, there are few studies of power-law slurries in rough fractures in grouting (Zhang 2013). El Tani (2012) made a theoretical analysis of cement diffusion based on the radial flow model in a planar fracture, obtained the theoretical formula of cement (Bingham), and the North American grouting method was reformulated in the field based on the GIN model. Sui *et al*. (2015) analyzed the diffusion path of chemical slurry (Newton) and its water plugging effect in the laboratory with a simplified glass planar model. Zhang *et al*. (2017) developed a calculation method of variable viscosity slurry (Newton) based on the planar model, and verified its accuracy of the calculation considering the slurry properties by using the experiment. From the studies, in the grouting field, the simple traditional theory should not be directly applied, and the theories and techniques should be developed for the grouting quality of the major projects. Through the recent theoretical, field and experimental results, it can be found that there are some limitations in the current research: generally based on planar or randomly constructed model assumptions. In addition, the shear can change the mechanical and hydraulic properties, and its effects cannot be carried out if based on the conventional models. So, a model of rough fracture should be established. Mu *et al*. (2019, 2020) verified the effects of roughness and spatial distribution in grouting engineering based on the slurry (Newton) properties obtained from the random rough model. To better guide the field engineering based on the theory, it is necessary to analyze the slurry diffusion according to the geological joints in engineering. Then, analysis of the hydraulic properties (Power-law) is worth based on the conventional roughness curves combined with numerical calculation, which can provide an effective guide for engineering.

For building rough fracture models, characterization and calculation methods of structural surface roughness have also been thoroughly studied, which are based on 10 standard roughness profiles proposed by Barton (Bae *et al*. 2011, Liu *et al*. 2017, 2019). It is more convenient to estimate JRCs by comparing the standard roughness for geological fractures. Considering grouting engineering, rough fracture models are established based on Barton standard structural planes using COMSOL™ Multiphysics computational fluid dynamics in this paper. The flow and diffusion of power-law grout with a low water-cement ratio in fractures and the hydraulic properties are analyzed, and a grouting parameter prediction model is established under standard roughness and is of great significance for guiding a grouting water shutoff project.

The organization for this research article is as follows. First, the methodology is presented. Then the results of diffusion-hydraulic properties in rough fractures were introduced, followed by the discussion and limitation. The summary and conclusions are finally highlighted.

2. Methodology

2.1 The rough fracture model and boundaries

Fluid always flows in the key control fracture in deep rock mass, which is affected by the fracture properties, such as wall bulge and undulation (Xiao *et al*. 2017, Mu *et al*. 2019). The wall properties can be defined by the JRC. According to the standard roughness profiles suggested by Barton and Choubey (1977), the roughness value is between 0 and 20 for natural rock mass structures, and any other roughness can be selected according to 10 standard contours. The roughness model can be used not only to calculate the strength of structural planes, but also to study

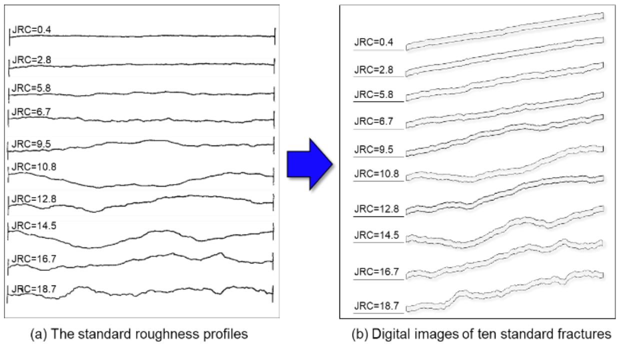

Fig. 2 Ten standard fracture models

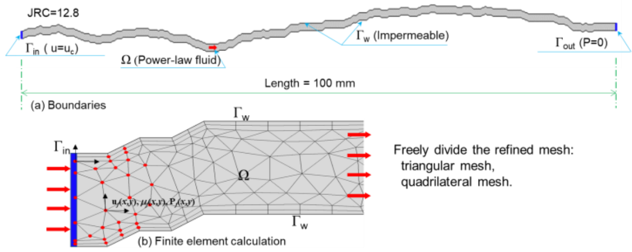

Fig. 3 The calculation boundaries of rough facture model

the mechanism of fluid diffusion in fractures (Koyama *et al*. 2008, Xie *et al*. 2015). A rough fracture model can be established by the ten standard roughness profiles (standard JRCs) to analyze the flow mechanism of power-law fluid. Ten standard roughness profiles are used to copy digital images by AutoCAD, of which there are no less than 400 copying points for each contour (Liu *et al*. 2017). Fracture models of different widths can be obtained after the specified translation distance occurs, as shown in Fig. 2. In addition, shear models can be generated by moving the lower fracture wall left.

For the model boundaries consisting of $\boldsymbol{\Gamma}_{in}$ Γ_{out} $\boldsymbol{\Gamma}_{w}$, $\boldsymbol{\Gamma}_{in}$ is at the left of the model with a constant flow rate ($u=u_c$), $\boldsymbol{\Gamma}_{out}$ is at the right of the model with a constant pressure (P=0), and $\boldsymbol{\Gamma}_{w}$ represents the two walls of fractures that are assumed to be impermeable and neglecting the seepage in deep intact rock mass. The diffusion domain $\boldsymbol{\Omega}$ is a fracture of length 100 mm and width based on the standard JRCs. The power-law fluid flow in the domain is limited to the given boundaries. One expression of the simulation model and boundaries is shown in Fig. 3. According to the principle of finite elements, the rough fracture can be divided into some triangular or quadrilateral elements, and every element has six or eight DOF. Every mechanical parameter ($\mathbf{u}_f(\mathbf{x,y})$, $\boldsymbol{\mu}_f(\mathbf{x,y})$, and $\mathbf{P}_f(\mathbf{x,y})$) of the grout slurry passes from the first force element to others.

2.2 Governing equations

Cement-based slurries with different water-cement ratios (W/C) have variable hydraulic properties. Based on previous research (Liu *et al*. 2018), a cement slurry with W/C = 0.5 can be expressed as a power-law fluid $\tau = m\gamma^n$, where τ is the shear stress, m is the power law coefficient, and n is the power law index. The rheological curves and fitting equations can be tested by a rheological experiment.

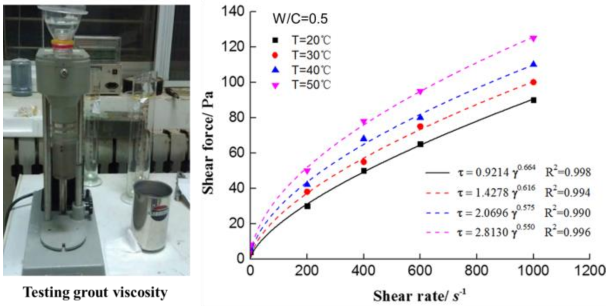

Fig. 4 Rheological equations for cement slurry with W/C = 0.5 (Liu *et al.* 2018)

In addition, the power law coefficient is a parameter related to temperature, as shown in Fig. 4. The slurry rheological parameters at room temperature (T=20°C) were selected as the main object in this study.

According to a stress analysis of the fluid micro elements, the equation of motion for the viscous fluid is expressed by the Navier-Stokes equation. After the pressure is introduced, the equation of motion and boundary conditions of the viscous fluid in the model can be obtained as follows:

$$\left.\begin{aligned} \rho_{\mathrm{f}}\frac{\mathrm{D}\mathbf{u}_{\mathrm{f}}}{\mathrm{Dt}} &= \rho_{\mathrm{f}}\mathbf{f}-\nabla \mathrm{p}+\nabla\cdot\boldsymbol{\tau} \quad \text{in } \boldsymbol{\Omega} \\ \mathbf{u} &= \mathbf{u}_{\mathrm{c}} \text{ on } \boldsymbol{\Gamma}_{\mathrm{in}} \\ \mathbf{P} &= \mathbf{0} \text{ on } \boldsymbol{\Gamma}_{\mathrm{out}} \\ \mathbf{u} &= \mathbf{0} \text{ on } \boldsymbol{\Gamma}_{\mathrm{w}} \end{aligned}\right\} \tag{1}$$

Based on the law of mass conservation, the continuity equation of the viscous flow control body can be obtained as follows:

$$\frac{D\rho_f}{Dt}+\nabla\cdot(\rho_f\mathbf{u}_f)=0 \tag{2}$$

It is generally assumed that the slurry is an incompressible fluid and that the density of the fluid is constant. Thus, the continuity equation can be simplified as:

$$\mathrm{div}\mathbf{u}_f=0 \tag{3}$$

According to Fig. 4, considering the conditions of the simulation calculation, the rheological parameters of a power-law fluid in a normal temperature environment are selected for analysis: m = 0.92 and n = 0.66, and the rheological equation can be illustrated by Eq. (4), where 2D and $\dot{\gamma}$ can be expressed by Christopher (1994) as follows:

$$\boldsymbol{\tau}=\mu(2\mathbf{D})=0.92\dot{\gamma}^{0.66-1}(2\mathbf{D}) \tag{4}$$

$$\left.\begin{aligned} 2\mathbf{D} &= (\nabla\mathbf{u}_f)^T+\nabla\mathbf{u}_f=\begin{pmatrix} 2\dfrac{\partial u_x}{\partial x} & \dfrac{\partial u_x}{\partial y}+\dfrac{\partial u_y}{\partial x} \\ \dfrac{\partial u_y}{\partial x}+\dfrac{\partial u_x}{\partial y} & 2\dfrac{\partial u_y}{\partial y} \end{pmatrix} \\ \dot{\gamma} &= \sqrt{\left|\frac{1}{2}\left[(\mathrm{tr}(2\mathbf{D}))^2-\mathrm{tr}((2\mathbf{D})^2)\right]\right|}=\sqrt{\left|4\left(\frac{\partial u_x}{\partial x}\frac{\partial u_y}{\partial y}\right)-\left(\frac{\partial u_x}{\partial y}+\frac{\partial u_y}{\partial x}\right)^2\right|} \end{aligned}\right\} \tag{5}$$

Eqs. (1)(3)- (5) are the governing equations of the slurry flow in the rough fracture model, which is a complex set of partial differential equations. Different models can be established based on the research conditions and standard roughness profiles, which can be illustrated as follows:

$$\left[PLFLOW-MODEL\right]=\begin{bmatrix} JRC \\ 0.4 \\ 2.8 \\ 5.8 \\ 6.7 \\ 9.5 \\ 10.8 \\ 12.8 \\ 14.5 \\ 16.7 \\ 18.7 \end{bmatrix}\times\begin{bmatrix} b_e \\ 0.5 \\ 1.0 \\ 1.5 \\ 2.0 \\ 2.5 \end{bmatrix}\times\begin{bmatrix} m & n \\ 0.92 & 0.66 \end{bmatrix}$$

3. Diffusion-hydraulic properties in rough fractures

3.1 Model verification

In order to verify the feasibility of using COMOL-CFD model to calculate slurry diffusion, the results obtained from Zhang (2017) experiment were compared and verified, as shown in Fig. 5. In this experiment, the transparent glass plate with grouting holes is used to form cracks, and the pressure sensor is used to monitor the grouting pressure in real time. The results of this experiment are shown in Fig. 5(a). The pressure variation curve of short-distance diffusion at the initial stage of grouting is compared with that calculated by COMSOL-CFD model. The variation characteristics of grouting pressure at different viscosity are also calculated under the same conditions. The comparison results are shown in Fig. 5(b). It can be seen from the figure that the calculated results of the model are basically consistent with the experimental results, and the CFD module can well reflect the hydraulic properties of slurry diffusion in fractures.

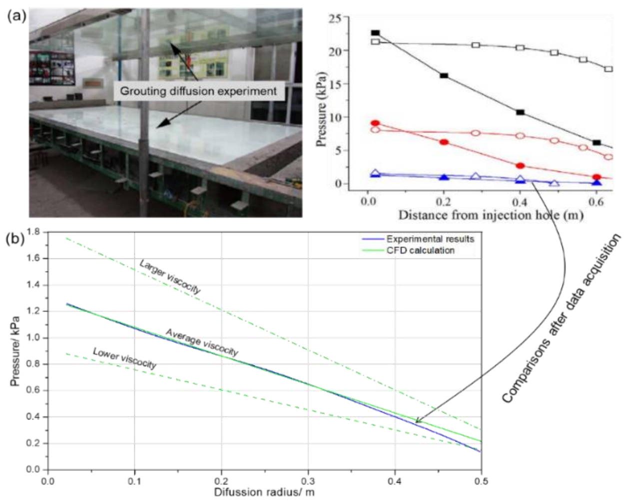

Fig. 5 Comparisons between calculation and experimental results

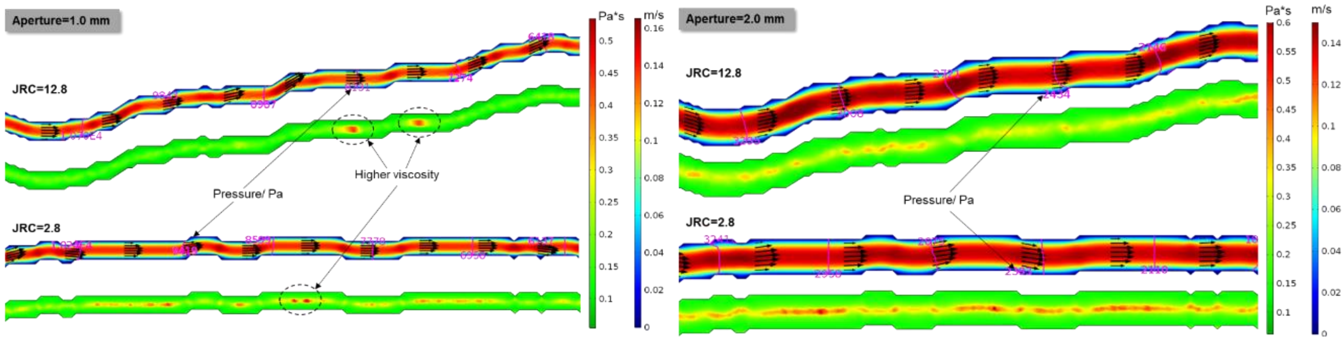

Fig. 6 Slurry flow properties in fractures

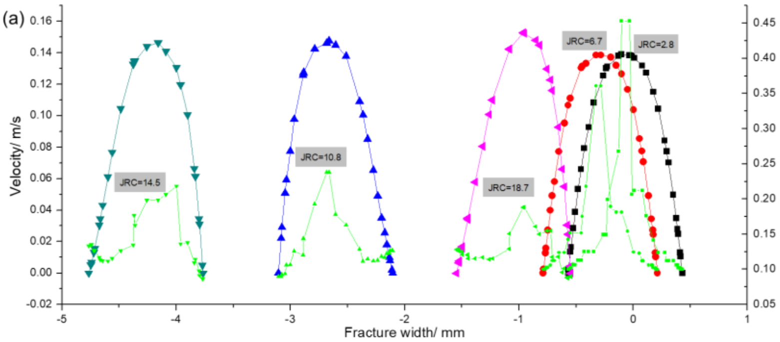

(a) Velocity and viscosity for different JRCs and the same width

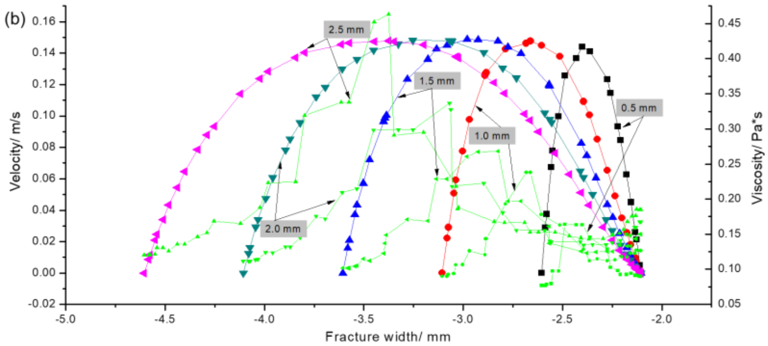

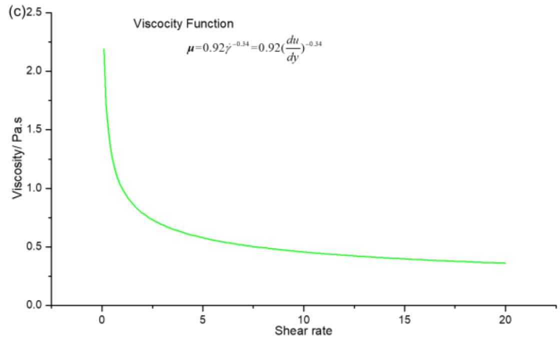

(b) For the same JRC and different widths (c) Viscosity function of the slurry

Fig. 7 Velocity and viscosity under different conditions, where green represents the curve of variable viscosity and others represent velocity

3.2 Pressure, velocity, and viscosity distributions

The digital standard roughness fracture model is imported into COMSOL from AUTOCAD. The power law slurry is calculated by the computational fluid module, and the grout diffusion flow properties can be analyzed after data processing. Based on the JRC and fracture aperture, fifty analyzed units were built. The pressure, velocity, and viscosity nephogram corresponding to fractures constructed by typical JRCs (2.8, 12.8) and fracture apertures (1.0 mm, 2.0 mm) are shown in Fig. 6.

As shown in Fig. 6, the pressure, velocity, and viscosity distributions are different for different JRCs and fracture widths. For fractures with the same apparent width, an increase in roughness leads to an increase in pressure; for the same JRC, an increase in fracture width leads to a decrease in pressure, which is also consistent with the theoretical calculation results by Rafi and Stille (2015). This type of grouting requires a high grouting pressure for diffusion in narrow and rougher fractures, which is the same as previous analysis (Liu *et al*. 2018). In addition, the pressure gradient of a power-law fluid is distinctly differentiated by the change in fracture strike pressure in a specific rough fracture with increasing fracture width, and the effect of the JRC becomes weaker. The maximum value of viscosity generally occurs in the place where the wall is smooth, and the relationship between velocity and viscosity can be explained by the smaller change rate of velocity leading to a larger value of viscosity in the adjacent region after a zigzag. The viscosities of power-law fluids show spatial distribution characteristics related to fractures in the diffusion, which are affected by the fluctuation and tortuosity of fracture walls. In addition, fractures with large wall variation (greater roughness) require higher grouting pressure. In large fractures, water plugging is more easily realized for low water-cement ratios because of higher viscosity

As shown in Fig. 7(a) and 7(b), the maximum viscosity

Table 1 Pressure gradient calculation and comparison

Fracture width/ mm	0.5	1.0	1.5	2.0	2.5
Gradient in smooth fracture/ Pa/ mm	-441.05	-140.19	-71.52	-44.63	-31.48
Calculated gradient with different JRCs Pa/ mm	-472.63	-147.03	-73.87	-45.59	-31.76
	-495.95	-152.41	-76.06	-46.65	-31.85
	-506.93	-154.53	-77.29	-47.19	-32.28
	-534.36	-161.09	-79.59	-48.49	-33.13
	-550.99	-165.84	-81.84	-49.56	-33.78
	-540.36	-163.40	-81.35	-49.49	-33.67
	-528.72	-163.57	-81.52	-49.90	-33.99
	-601.16	-183.07	-89.15	-53.93	-36.95
	-604.11	-180.97	-89.36	-53.95	-36.73
	-684.01	-202.00	-97.86	-59.04	-39.81

distribution occurs at the maximum velocity of slurry flow, that is, the middle part of the fracture width. Under the same roughness condition, the maximum rate does not change obviously, but the viscosity increases with increasing fracture width. The viscosity of the low water-cement ratio slurry (pseudo plastic fluid) is the highest in the middle of the fracture, which is consistent with the theoretical viscosity function of the slurry, as shown in Fig. 7(c), and the viscosity increases with decreasing shear rate. When there is water flow in the fissure (grouting to block seepage), the velocity of water in the middle of the fissure is usually the largest. Thus, this is the reason that water is always blocked by low water-cement ratio grout and then filled with other types of slurry, such as chemical slurry, which easily diffuses and flows in narrow fissures.

3.3 Response of JRCs for pressure gradient

Based on the results of COMSOL simulations, the pressure distribution along the length can be obtained. The gradient of pressure drop data can be fitted by the diffusion radius, and the detailed calculated results are illustrated in Table 1.

For the pressure gradient, to make the results more obvious compared to a smooth fracture and eliminate the defects of computing, the smooth models were calculated for the same aperture using the governing equations. The calculation results are compared using dimensionless values as follows:

$$DV = \frac{\mathbf{J}_{i,j}}{\mathbf{J}_{i,0}} \tag{6}$$

For a fracture with typical rough structural surface, the pressure gradient growth rate (DV) can basically be divided into three stationary zones by JRC ranges (JRCs < 5.8, 9.5 < JRCs < 12.8, 14.5 < JRCs < 16.7) and three transition zones (5.8 ≤ JRCs ≤ 9.5, 12.8 ≤ JRCs ≤ 14.5, JRCs >16.7). However, as the fracture width decreases, the plateau will be broken and changed, and a mutation domain will occur in the second plateau (10.8, 12.8). When the fracture width is less than 1.5 mm, increased catastrophe slopes will occur in this region ($|\alpha 1|>|\alpha 2|>|\alpha 3|$), and as shown in Fig. 8, with

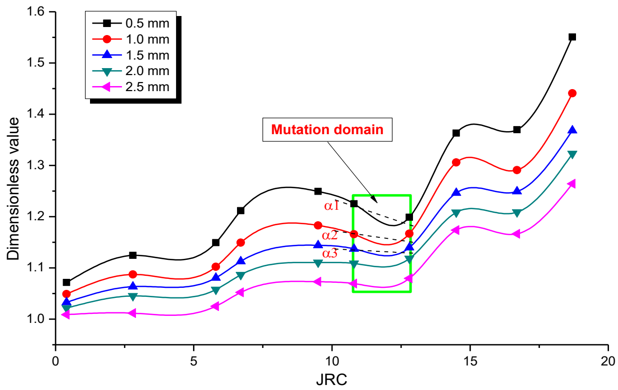

Fig. 8 Trend of the pressure gradient with JRCs in fractures

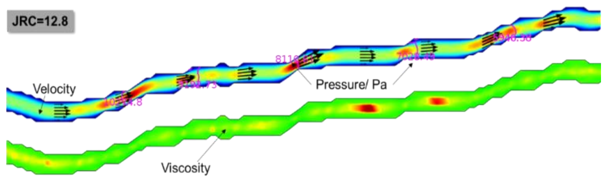

Fig. 9 The hydraulic parameters with SD

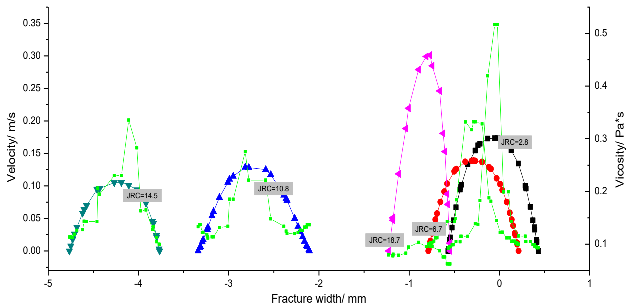

Fig. 10 Velocity and viscosity with SD for different JRCs

decreasing fracture width, the classification is significantly affected by the roughness.

For the JRCs proposed by Barton (1977) ranging from 10.8 to 12.8, there are large fluctuations in the 10 cm length; however, the partial fracture wall is relatively smooth, and the protrusion on the surface has a greater impact on the pressure. As the fracture width decreases, the wall bulge effect increases, resulting in a sudden change zone when the influence value is smaller than other roughness values. Therefore, the JRC effects on the grouting pressure gradient correspond to the width, and the smaller the gap width is, the worse the regularity. In addition, as shown in Fig. 8, when the roughness is less than 10.8, and the pressure gradient changes slightly with increasing roughness. But it changes significantly when the roughness is greater than 10.8. The effects of small apertures and moderate to larger roughness (JRCs > 10.8) on the permeability of independent surfaces cannot be underestimated.

3.4 Effects of shear displacement (SD)

Influenced by varying apertures caused by shear displacement (SD), the slurry velocity in the fracture increases, and it causes the viscosity deviation to increase.

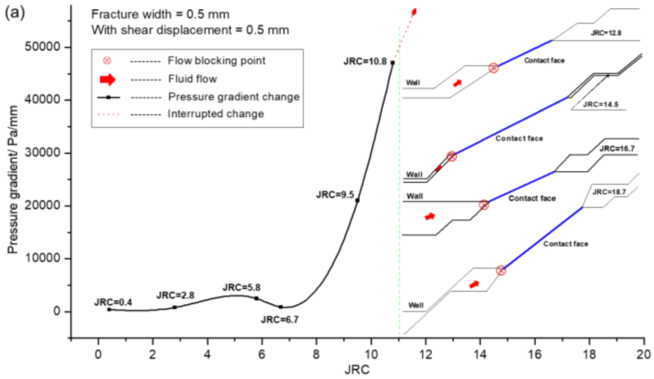

(a) Numerical fracture with SD

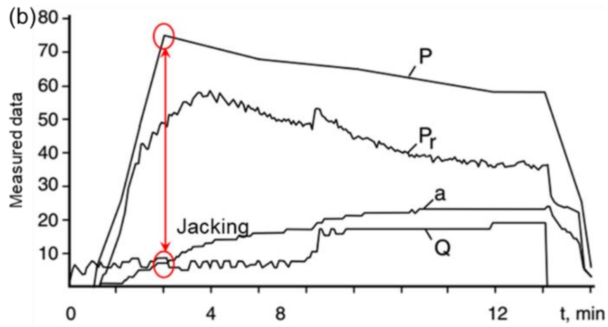

(b) Measured data (Gothall and Stille 2009)

Fig. 11 Numerical and geological fracture grouting

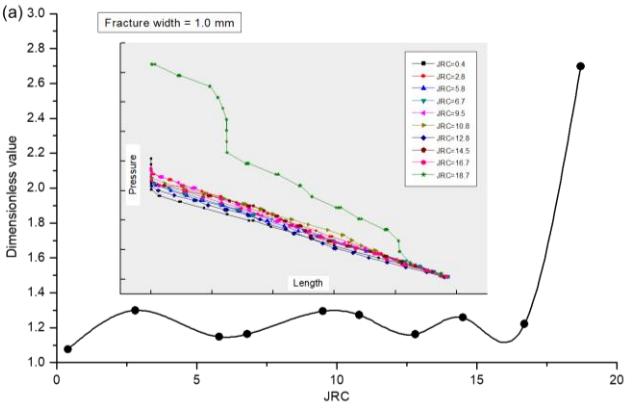

(a)Numerical fracture with shear

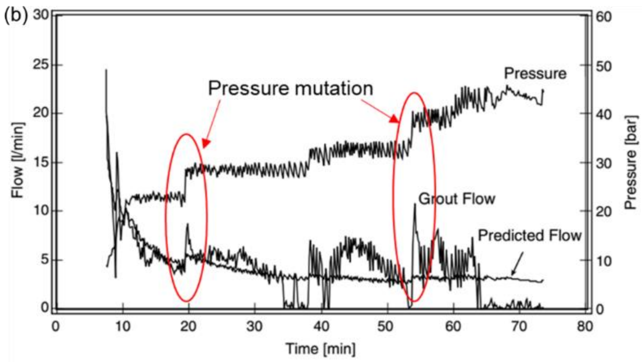

(b) Pumping data measured (Gothall and Stille 2009)

Fig. 12 Pressure variation of a connected fracture along the whole length

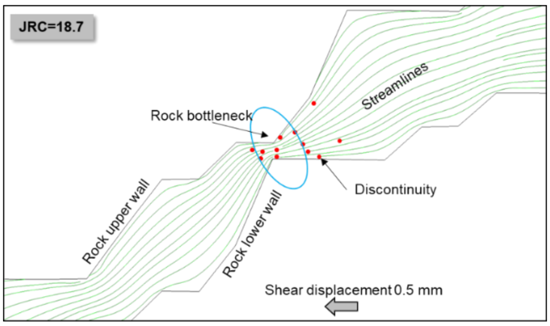

Fig. 13 Streamline distribution in the cliff-like change area

In the narrow part of the fracture, the velocity is larger, but the viscosity is smaller. The slurry has high-viscosity points in the middle parts of relatively smooth areas but smaller in other zones. The shear movement causes a sudden increase in the pressure value of high-roughness fractures, which changes the original distribution.

As shown in Figs. 9 and 10, the maximum viscosity distribution also occurs at the middle part of the fracture, and the average viscosity is smaller. More accelerator dosage should be added to lower W/C slurry to achieve a better water plugging effect in the rougher fractures.

By analyzing the gradient increment caused by the roughness after the shear displacement in a 1 mm fracture (the lower joint profile shear moves 0.5 mm left), it can be found that the shear does not change stationary zones, but expands to a single floating stationary zone (JRCs < 16.7), as shown in Fig. 11(a). Affected by shear displacement, under high roughness conditions (JRCs > 16.7), the pressure gradient increases significantly, in contrast, under other medium and low JRC conditions (JRCs < 16.7), the values fluctuate within a certain range.

After shear movement, as illustrated in Fig. 11, the pressure gradient shows some changes in fissures with different apertures. For a narrow fracture (b = 0.5 mm), at medium and low JRCs, a trend of exponential growth appears after stabilization, but the fitting degree of the pressure gradient is approximately less than 90% or even 60% because of the cliff-like changes. For larger roughness (JRCs > 10.8), the contact surfaces are generated to prevent the diffusion of grout because of the wall fluctuation. The effects of small apertures and moderate to larger roughness (JRCs > 10.8) are greater. The grouting pressure will continue to increase before the first contact surface until the fracture surface is jacked, damaged and split (Gothall and Stille 2009), as shown in Figs. 11(a) and 11(b). Different rough fractures have fluid blocking points at different locations, such as for JRC = 12.8 at 35 mm, 14.6 at 50 mm, 16.7 at 51.5 mm and 18.7 at 23.4 mm, which cause pressure mutation. For other fractures (b ≥ 1.0 mm) with SD = 0.5 mm there are cliff-like changes instead of fluid blocking points in whole roughness profiles with higher fitting degrees.

For fissures with larger apertures, shear displacement

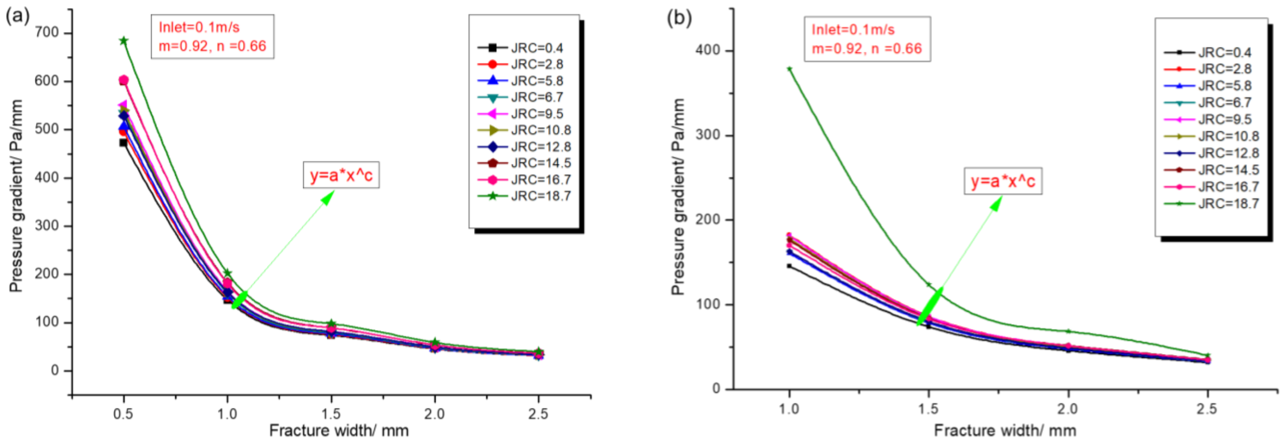

(a) Pressure with NSD (b) Pressure with SD of 0.5 mm

Fig. 14 The fitting curves of the pressure gradient

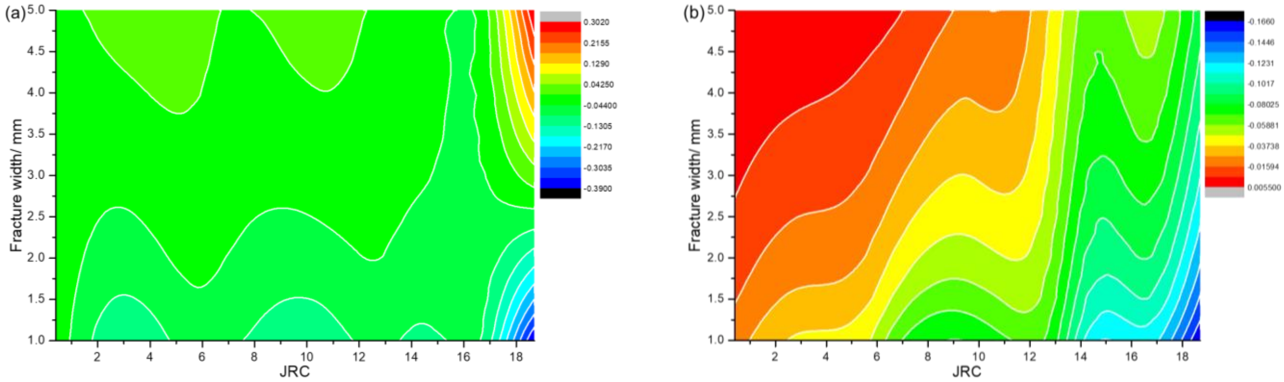

(a) Deviation rate with SD (a) Deviation rate with NSD

Fig. 15 The deviation rate under different conditions

Table 2 Best fit equations for standard JRC profiles

Barton-JRC	Standard profiles		Best fit equations		Aperture/ mm	
			NSD	SD lower R^2	NSD	SD lower R^2
0-2 (0.4)			$146.93b_e^{-1.686}$	$145.59b_e^{-1.667}$	$0.978b_e^{1.017}$	$0.981b_e^{1.007}$
2-4 (2.8)			$152.19b_e^{-1.704}$	$182.03b_e^{-1.829}$	$0.961b_e^{1.026}$	$0.878b_e^{1.088}$
4-6 (5.8)			$154.64b_e^{-1.713}$	$160.79b_e^{-1.750}$	$0.951b_e^{1.030}$	$0.934b_e^{1.050}$
6-8 (6.7)			$160.99b_e^{-1.731}$	$162.96b_e^{-1.744}$	$0.934b_e^{1.040}$	$0.928b_e^{1.046}$
8-10 (9.5)		$\mathbf{J}_{i,j} = ax^c =$	$165.60b_e^{-1.734}$	$181.33b_e^{-1.826}$	$0.920b_e^{1.041}$	$0.880b_e^{1.087}$
10-12 (10.8)			$163.49b_e^{-1.725}$	$178.08b_e^{-1.822}$	$0.927b_e^{1.037}$	$0.888b_e^{1.085}$
12-14 (12.8)			$162.94b_e^{-1.698}$	$162.75b_e^{-1.735}$	$0.927b_e^{1.023}$	$0.929b_e^{1.042}$
14-16 (14.5)			$181.59b_e^{-1.728}$	$175.86b_e^{-1.781}$	$0.879b_e^{1.038}$	$0.893b_e^{1.065}$
16-18 (16.7)			$180.87b_e^{-1.740}$	$170.15b_e^{-1.740}$	$0.882b_e^{1.044}$	$0.908b_e^{1.044}$
18-20 (18.7)			$201.34b_e^{-1.765}$	$377.28b_e^{-2.594}$	$0.834b_e^{1.057}$	$0.610b_e^{1.471}$

will not lead to the occurrence of a contact surface but rather a bottleneck under standard roughness. As shown in Fig. 12(a), in a fracture with 1 mm width, a move displacement of 0.5 mm makes the pressure greater than the previous one. However, the pressure drop is linear except for JRC = 18.7. The shear movement makes the fluid diffusion change significantly or appears to reach a singularity. The effect of roughness becomes more important under SD than for aperture. Under high roughness (JRC = 18.7), there is a cliff-like change area in the pressure gradient, which reveals the sudden change in pressure of the actual grouting on site, as shown in Fig. 12(b). According to the fracture geometry, the change area is caused by the narrow zone (rock bottleneck) in the fracture because of the shear movement of 0.5 mm, as shown in Fig. 13.

Numerical calculations indicate that the spread of grout could be a mean value process reflecting the rheological properties of grout but that depends on the penetrability in terms of its weakest link. As shown in Fig. 13, there are some discontinuities for streamlines with the same flow density in this region, i.e., the fluid converges to a small number of streamlines passing through a rock bottleneck and the pressure increases greatly. In addition, the fluid viscosity is very small, and the velocity will increase abnormally. Because of the influence of shear movement, there are different rock bottlenecks in the direction of fracture diffusion. The response of different roughness and fracture apertures to shear displacement are different, and the responses of small apertures and higher JRCs are strong. Grouting parameters are divided into several sections, which are affected by crack bottlenecks and breakpoints due to wall fluctuation and shear movement.

3.5 Best fit for standard JRCs

The slurry element in the center of a fissure can be selected to analyze the stress state. In a position with a grouting radius of r, the gradient of slurry velocity can be expressed as follows (Zhang *et al*. 2017):

$$\frac{dv}{dw_e} = \frac{w_e}{\mu}(\mathbf{J}_b) \tag{7}$$

Considering the assumption that the velocity of the fracture wall is 0, the average slurry velocity in the grouted zone can be expressed as:

$$\overline{v} = \frac{1}{b_h}\int \frac{w_e}{\mu}(\mathbf{J}_{i,j}) = \frac{b_h^{\,2}}{12\overline{\mu}(m,n)}(\mathbf{J}_{i,j}) \tag{8}$$

In practical grouting engineering, a simple formula is usually used to calculate grouting pressure, which is related to the average viscosity, average velocity and hydraulic aperture (Zhang *et al*. 2017). The pressure gradient can be obtained based on Eq. (8) as follows:

$$\mathbf{J}_{i,j} = 12\overline{\mu}(m,n)\overline{v}b_h^{-2} \tag{9}$$

To study the influence of roughness and apparent fissure width on hydraulic parameters (hydraulic fracture width), different models were calculated under a 0.1 m/s inlet conditions. The fitting curves of the NSD and SD models are shown in Fig. 14. When affected by roughness, the fitting curves show a gentle difference distribution with NSD but have a larger deviation for a JRC of 18.7 with SD. According to the fitting curves shown in Fig. 14, the fitting formula corresponding to the Barton-JRC can be obtained.

$$\mathbf{J}_{i,j} = a(b_e)^c \tag{10}$$

Under the conditions of NSD or SD in larger fractures, the hydraulic aperture can be calculated with the assumptions of average velocity and viscosity as follows:

$$b_h = \sqrt{\frac{12\overline{\mu}(m,n)\overline{v}}{\mathbf{J}_{i,j}}} = \sqrt{\frac{12\overline{\mu}_e(m,n)\overline{v}_e}{a(b_e)^c}} \tag{11}$$

By eliminating model errors and substituting a smooth fracture into the relationship between calculated and theoretical fracture width, the hydraulic aperture can be obtained. For the smooth fracture model, the fitting equation is as follows:

$$\mathbf{J}_{i,j} = 140.29b_e^{-1.652} = 12\overline{\mu}\overline{v}b_e^{-2} \tag{12}$$

Thus, the assumed average viscosity and flow rate can be expressed by the geometrical aperture as follows:

$$\sqrt{\overline{\mu}\overline{v}} = 3.42b_e^{0.174} \tag{13}$$

Based on Eqs. (10) and (13), the best fit equations and hydraulic aperture can be obtained under the conditions of NSD and SD considering the average estimated parameters (average aperture, *m*, and *n*) in grouting engineering, as illustrated in Table 2.

Roughness and shear movement change the hydraulic aperture. When designing the grouting parameters in engineering, the grouting aperture in Table 2 should be used for calculation, which also provides an effective method of calculating hydraulic grouting aperture for various kinds of slurry. As shown in Table 2 and Fig. 14, the influence of standard roughness decreases with increasing fracture width, which can be neglected after reaching a certain value of 2.5 mm, but it plays a key role in narrow fractures. The influence of roughness is limited by the fracture aperture threshold. The grouting fluidity and groutability of the main rock mass are jointly determined by the aperture and roughness.

In view of the change of hydraulic radius caused by the change of roughness in grouting, the deviation rates of smooth plate cracks and different JRCs are compared, as shown in Fig. 15. Under the same JRC condition, the deviation rate decreases with the increase of the aperture of the crack when the crack does not shear, while when the roughness is less than 10, the deviation rate increases obviously with the increase of the roughness; but when the deviation rate is greater than 10, the deviation rate fluctuates greatly, showing a multi-hump-like change. And all fracture widths are smaller (negative growth). However, the distribution of the deviation rate varies greatly after the shear movement of the crack. The deviation rate increases with the fracture width increasing after 3.0 mm when JRC is smaller than 16. When the roughness is greater than 16, there are positive and negative symmetrical distributions of deviation rates with the centerline of 2.5 mm. The dual effects of shear movement and roughness play an important role in fracture permeability.

4. Case studies of water plugging

A power-law slurry has a larger viscosity and always solidifies easily in the middle, as shown in Fig. 16(a). If the slurry is first solidified in the middle, the lower water flow velocity can also be affected by the rough fracture wall. The high viscosity slurry ratio in the middle of the wall easily blocks the flow, whereas the flow diffusing to the wall changes the streamline under the action of the rough wall (as shown in Fig. 16(b)); the effective fracture width of the main streamlines decreases, which more easily achieves water plugging. It is easier to achieve a water plugging effect by using this kind of slurry for grouting plugging.

Based on the above hydraulic characteristics of low water-cement ratio grout in rough fractures, reducing the water-cement ratio is critical to improving the stone rate, the stability of the slurry and the stone strength; thus, the water-cement ratio should be decreased as much as possible under the conditions that injection is maintained and time is allowed when grouting. Rapid condensation and water plugging can easily be realized in short-distance and large-width fractures. This mechanism also explains the application principle of slurries with low water-cement ratios in practical production.

Case 1: An underwater highway tunnel in China (Cui 2011)

The tunnel crosses rivers and takes measures to prevent water gushing and landslides during construction, actively carries out water exploration grouting and reinforces surrounding rock, as shown in Fig. 17. A large amount of water gushing occurred in the 7th hole of the second west section of the tunnel approximately 2 hours after drilling. According to the drilling data and the water output, there is a water-bearing gravel and sediment layer at a depth of 40 m, with large fissures, good connectivity and large slurry absorption in tunneling engineering.

In the initial stage, the slurry with a water-cement ratio of 0.8~1:1 was used. However, in the process of grouting, the conveying capacity of equipment was limited, the pressure could not be increased for a long time, and water plugging was not fully realized. Later, the slurry of 0.5~0.6:1 with high concentration sodium silicate was used to increase the slurry concentration and shorten the gelling time, and intermittent grouting was adopted to block the large outflow borehole. After two hours, the water gushing from the borehole was blocked.

Case 2: Huangsha Station of Guangzhou Metro Line 1 in China (Cui 2011)

The foundation pit excavation elevation of the station is basically aquifer, and the groundwater level is 1.5~2.0 m below the surface and is quite abundant. A cement slurry with a water-cement ratio of 0.3~0.9:1 was used to plug underground water leakage by grouting, and a large area water leakage was successfully controlled.

Case 3: Grouting of working face in No.1 coal of Zhangji Coal Mine

Mining No.1 coal in Zhangji Coal Mine is threatened by water hazards from the floor aquifer. In order to ensure safety in production, grouting operation is carried out. The cement slurry with water-cement ratio of 1.0:1 is still used. However, for extensively faulted region, the slurry running occurs in the later stage and the water inflow of borehole remains stable without decreasing. In order to solve these problems, the water flow conditions and the dilution of coarse grains between faults are analyzed, and the stage grouting is recommended. In the initial stage, the cement-based slurry with low-water cement ratio of 0.5:1 was used and the accelerator was added to deep high-pressure grouting.

According to the calculation formula considering roughness, the grouting aperture was preliminarily estimated to design the effective grouting parameters. In the later stage, higher-water cement ratio of 1.0:1 was used. After the improvement of the project, the fault fissures are gradually filled and the strength of rock mass is continuously improved. Experiential directional long borehole verification shows that the water inflow is effectively controlled, as shown in Fig. 18.

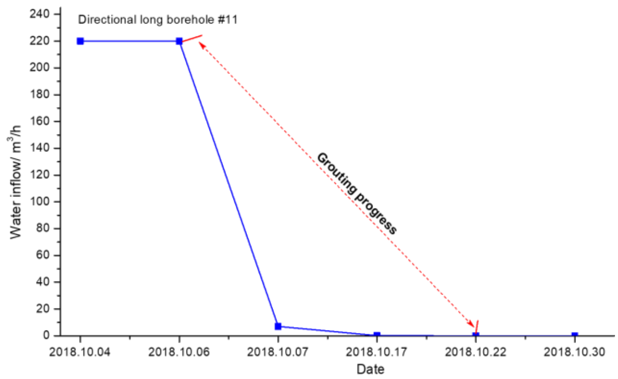

Fig. 18 Variation of water inflow with time

Low water-cement slurries are used in water plugging and seepage control engineering cases. One of the plugging principles is that the slurry follows a power-law fluid model and is pseudo plastic. In the middle of fissures and boreholes, the slurry will show larger viscosity, which is conducive to the avoidance of high-speed water flow. Additionally, with the function of rough walls, solidified cement partials, and accelerated solidification of additives, water plugging can be achieved. Under a high-water condition, a cement-based slurry with a high water-cement ratio cannot achieve water plugging because its flow pattern is often Newtonian (Liu *et al.* 2018), and the viscosity distribution is identical in fracture sections, so superior plugging by the slurry cannot be achieved. In view of the phenomena of shear movement and particle filling in shallow rock mass fractures, an accelerator should be added according to the complexity of fractures when using lower water-cement ratio slurry.

5. Discussion and limitation

The power law characteristics of slurries with low water-cement ratios are one of the reasons for achieving better water plugging. However, in engineering, additives with different proportions are always mixed with slurries in conditions of massive water. Additives can change the hydraulic coefficients m and n of slurries at low water ratio, and even change the flow patterns of slurries (Eriksson *et al.* 2004, Zhang *et al.* 2017). Therefore, additive materials should be deeply studied, especially for the flow mechanism of various water shutoff materials in complex geological conditions.

Based on the flow pattern study of slurry with a specific water-cement ratio, the hydraulic properties calculated in this paper can be used in grouting engineering, and are also helpful in revealing the grouting mechanism of water-cement ratio slurry. However, on basis of analysis carried out in this study, the available literature, and the current trends of engineering practice, fractured rock masses have variable shear movements. Shear will cause more contact points and contact surfaces on the internal surface of a fracture, which will have a serious impact on the slurry diffusion. The 2D calculation results considering the fluctuation of fracture wall and power-law flow pattern have guiding significance for grouting engineering. However, the combination of real-time digital imaging and numerical simulation of grouting fracture surfaces in tunneling is one of the keys to solve the problem of water plugging engineering in real time.

According to the analysis in this paper, shear movement in larger fissures results in a cliff-like drop in the pressure gradient, but an increase in the fracture width leads to a decrease in this response. In narrow fissures, there are some blocking points instead of the cliff-type zones, which is the main factor that causes the sustained rise of grouting pressure and fracture dilation to damage splitting. The research on the connectivity of contact surface or discontinuous fractures has also become one of the key problems in optimizing grouting.

The analysis of hydraulic properties for power-law fluid, rock fracture roughness, and shear movement can not only be used to guide the design of grouting engineering parameters, but also proppant migration, fracturing fluid diffusion, and extraction in oil and gas reservoir development engineering (Omosebi and Igbokoyi 2016, Dejam 2018). The mechanisms of flow, jacking and splitting of power-law variable fluid in geological fissures under different confining pressures should be further studied.

In this study, the standard JRCs are applied in the grouting models. The hydraulic properties of the power-law slurry commonly used for water plugging are analyzed. The grouting mechanism in the rough fracture is further obtained, which is effective for the optimization of engineering parameters. The calculation results are based on the model of two-dimensional conditions. However, the slurry flow in the geological fracture is a random multi-directional three-dimensional spatial form, so the research on the structural roughness has gradually developed to three-dimensional. And the external conditions of the fracture, such as shear movement, are variable and multidirectional. There are some limitations in this study: the fluid is assumed to be homogeneous in a single flow direction and the interaction of mud particles is ignored. The slurry flow is simulated in the connected domain without considering the non-connected breakpoints caused by the contact points of convex walls. Also, the breakpoints can cause continuous pressure holding and matrix expansion or even splitting, and the hydraulic changes caused by it are neglected. The limitations of theory and simulation in this study will be the future research topic.

6. Conclusions

In this paper, a flow-diffusion model of power-law slurry in rough fractures is built based on the Navier-Stokes equations and standard roughness (JRC) profiles proposed by Barton. Ten standard structural planes for JRCs from 0.4 to 18.7, fracture apertures from 0.5 to 2.5 mm, and shear movement of 0.5 mm were used to analyze the flow mechanism.

- The pressure, velocity, and viscosity distributions are affected by the values of JRCs and fracture width. The maximum viscosity is distributed at the maximum velocity of the slurry flow. The maximum velocity does not change as the fracture width increases, but the viscosity increases. This is one of the reasons that water is always blocked by low water-cement ratio slurry in geological fractures.
- The whole process of standard roughness profiles can be divided into three stationary zones (JRCs < 5.8, $9.5 <$ JRCs < 12.8, $14.5 <$ JRCs < 16.7) and three transition zones ($5.8 \leq$ JRCs ≤ 9.5, $12.8 \leq$ JRCs ≤ 14.5, JRCs >16.7). The fracture models composed of 10 structural planes tend to change the pressure gradient between 10 and 14, which increases with decreasing fracture width. The effects of small apertures and moderate to larger roughness (JRCs > 10.8) on the permeability of independent surfaces cannot be underestimated. The influence of standard roughness can be neglected when the fracture width reaches a certain value.
- The hydraulic properties changed substantially after shear movement of 0.5 mm. The slurry has lower viscosity with higher velocity in the fracture. The pressure gradient has different cliff-like trends along the length with different JRCs and apertures. There are blocking points instead of cliff-like zones for narrow fractures, and pressure increases exponentially after stabilization for lower JRCs but with lower fitting degrees ($R^2 < 80\%$), and grouting is divided into several stages. The shear does not change stationary zones below 10.8, but expands to a single floating stationary zone.
- The fitting equations for different JRCs are obtained based on the calculations, which conform to a power-law model: $y=a^*(x)^c$, where c meets the conditions of $-2 < c < 0$. Considering the slurry stress state and boundaries, the hydraulic apertures are also obtained, and this approach provides an effective method for optimizing grouting parameters in engineering. The dual effects of shear movement and roughness play an important role in the effective hydraulic radius and permeability of the fracture.
- For grouting water plugging, the water-cement ratio, grouting pressure and grouting additives should be determined by combining the flow conditions and the apparent widths of the main fracture and rough surface. It is easier to plug water with low water-cement ratio slurry for fractures with larger wall tortuosity. The permeability coefficient calculated by flow alone cannot directly be used to estimate the amount of slurry. In engineering, it can be reasonably estimated by using the proposed method in accordance with the standard fracture structure proposed by Barton.

Acknowledgments

This work was conducted with support from the National Natural Science Foundation of China (grant nos.51879041, 51761135102 and U1710253), Fundamental

Research Funds for the Central Universities (No. N180105029), and Postdoctoral Science Foundation of China (grant no. 2018M641706). The authors express their sincere thanks to the reviewers for their helpful comments and suggestions for improving this paper.

References

Amadei, B. and Savage, W.Z. (2001), "An analytical solution for transient flow of Bingham viscoplastic materials in rock fractures", *Int. J. Rock Mech. Min. Sci.*, **38**(2), 285-296. https://doi.org/10.1016/S1365-1609(00)00080-0.

Bae, D.S., Kim, K.S., Koh, Y.K. and Kim, J.Y. (2011), "Characterization of joint roughness in granite by applying the scan circle technique to images from a borehole televiewer", *Rock Mech. Rock Eng.*, **44**(4), 497-504. https://doi.org/10.1007/s00603-011-0134-9.

Barton, N. and Choubey, V. (1977), "The shear strength of rock joints in theory and practice", *Rock Mech.*, **10**(1), 1-54. https://doi.org/10.1007/BF01261801.

Butron, C., Gustafson, G., Fransson, A. and Funehag, J. (2010), "Drip sealing of tunnels in hard rock: A new concept for the design and evaluation of permeation grouting", *Tunn. Undergr. Sp. Technol.*, **25**(2), 114-121. https://doi.org/10.1016/j.tust.2009.09.008.

Chang, X., Li, Z.H., Wang, S.Y. and Wang, S.R. (2018), "Pullout performances of grouted rockbolt systems with bond defects", *Rock Mech. Rock Eng.*, **51**(3), 861-871. https://doi.org/10.1007/s00603-017-1373-1.

Christopher, M. (1994), *Rheology Principles, Measurements, and Applications*, WILEY-VCH, New York, U.S.A.

Cui, J.J. and Cui, X.Q. (2011), *Grouting Technology for Tunnel and Underground Engineering*, China Construction Industry Publishing House, Beijing, China.

Dejam, M. (2018), "Dispersion in non-Newtonian fluid flows in a conduit with porous walls", *Chem. Eng. Sci.*, **189**, 296-310. https://doi.org/10.1016/j.conbuildmat.2017.01.031.

Dejam, M. (2019), "Advective-diffusive-reactive solute transport due to non-Newtonian fluid flows in a fracture surrounded by a tight porous medium", *Int. J. Heat Mass Transfer*, **128**, 1307-1321. https://doi.org/10.1016/j.ijheatmasstransfer.2018.09.061.

Dejam, M., Hassanzadeh, H. and Chen, Z.X. (2016), "Shear dispersion in a capillary tube with a porous wall", *J. Contam. Hydrol.*, **185**, 87-104. http://doi.org/10.1016/j.jconhyd.2016.01.007.

Dejam, M., Hassanzadeh, H. and Chen, Z.X. (2018), "Shear dispersion in a rough-walled fracture", *SPE J.*, **23**(5), 1669-1688. http://doi.org/10.2118/189994-PA.

El Tani, M. (2012), "Grouting rock fractures with cement grout", *Rock Mech. Rock Eng.*, **45**(4), 547-561. https://doi.org/10.1007/s00603-012-0235-0.

Eriksson, M., Friedrich, M. and Vorschulze, C. (2004), "Variations in the rheology and penetrability of cement-based grouts—an experimental study", *Cement Concrete Res.*, **34**(7), 1111-1119. https://doi.org/10.1016/j.cemconres.2003.11.023.

Funehag, J. and Gustafson, G. (2008), "Design of grouting with silica sol in hard rock–New methods for calculation of penetration length, Part I", *Tunn. Undergr. Sp. Technol.*, **23**(1), 1-8. https://doi.org/10.1016/j.tust.2006.12.005.

Gothall, R. and Stille, H. (2009), "Fracture dilation during grouting", *Tunn. Undergr. Sp. Technol.*, **24**(2), 126-135. https://doi.org/10.1016/j.tust.2008.05.004.

He, K.Q., Wang, R.L. and Jiang, W.F. (2012), "Groundwater inrush channel detection and curtain grouting of the Gaoyang iron ore mine, China", *Mine Water Environ.*, **31**(4), 297-306. https://doi.org/10.1007/s10230-012-0207-3.

Huang, Y.B., Zhang, Y.J., Yu, Z.W., Ma, Y.Q. and Zhang, C. (2019), "Experimental investigation of seepage and heat transfer in rough fractures for enhanced geothermal systems", *Renew. Energy*, **135**, 846-855. https://doi.org/10.1016/j.renene.2018.12.063.

Javadi, M., Sharifzadeh, M. and Shahriar, K. (2010), "A new geometrical model for non-linear fluid flow through rough fractures", *J. Hydrol.*, **389**(1-2), 18-30. https://doi.org/10.1016/j.jhydrol.2010.05.010.

Koyama, T., Neretnieks, I. and Jing, L. (2008), "A numerical study on differences in using Navier-Stokes and Reynolds equations for modeling the fluid flow and particle transport in single rock fractures with shear", *Int. J. Rock Mech. Min. Sci.*, **45**(7), 1082-1101. https://doi.org/10.1016/j.ijrmms.2007.11.006.

Liu, J.J., Wang, Y. and Song, R. (2017), "A pore scale flow simulation of reconstructed model based on the micro seepage experiment", *Geofluids*, UNSP 7459346. https://doi.org/10.1155/2017/7459346.

Liu, Q.S., Lei, G.F., Peng, X.X., Lu, C.B. and Wei, L. (2018), "Rheological characteristics of cement grout and its effect on mechanical properties of a rock fracture", *Rock Mech. Rock Eng.*, **51**(2), 613-625. https://doi.org/10.1007/s00603-017-1340-x.

Liu, X.G., Zhu, W.C., Yu, Q.L., Chen, S.J. and Guan, K. (2019), "Estimating the joint roughness coefficient of rock joints from translational overlapping statistical parameters", *Rock Mech. Rock Eng.*, **52**(3), 753-769. https://doi.org/10.1007/s00603-018-1643-6.

Liu, X.G., Zhu, W.C., Yu, Q.L., Chen, S.J. and Li, R.F. (2017), "Estimation of the joint roughness coefficient of rock joints by consideration of two-order asperity and its application in double-joint shear tests", *Eng. Geol.*, **220**, 243-255. https://doi.org/10.1016/j.enggeo. 2017.02.012.

Mu, W.Q., Li, L.L., Yang, T.H., Yao, L.J. and Wang, S.X. (2020), "Numerical calculation and multi-factor analysis of slurry diffusion in inclined geological fracture", *Hydrogeol. J.*, 1-18. https://doi.org/10.1007/s10040-019-02103-y.

Mu, W.Q., Li, L.L., Yang, T.H., Yu, G.F. and Han, Y.C. (2019), "Numerical investigation on a grouting mechanism with slurry-rock coupling and shear displacement in a single rough fracture", *Bull. Eng. Geol. Environ.*, **78**(8), 6159-6177. https://doi.org/10.1007/s10064-019-01535-w.

Niya, S.M.R. and Selvadurai, A.P.S. (2017), "The estimation of permeability of a porous medium with a generalized pore structure by geometry identification", *Phys. Fluids*, **29**(3), 037101. https://doi.org/10.1063/1.4977444.

Niya, S.M.R. and Selvadurai, A.P.S. (2019), "Correlation of joint roughness coefficient and permeability of a fracture", *Int. J. Rock Mech. Min. Sci.*, **113**, 150-162. https://doi.org/10.1016/j.ijrmms.2018.12.008.

Omosebi, A.O. and Igbokoyi, A.O. (2016), "Boundary effect on pressure behavior of power-law non-Newtonian fluids in homogeneous reservoirs", *J. Petrol. Sci. Eng.*, **146**, 838-855. https://doi.org/10.1016/j.petrol.2016.07.036.

Ozsun, O., Yakhot, V. and Ekinci, K.L. (2013), "Non-invasive measurement of the pressure distribution in a deformable micro-channel", *J. Fluid Mech.*, **734**, R1. https://doi.org/10.1017/jfm.2013.474.

Qian, Z.W., Jiang, Z.Q., Guan, Y.Z. and Yue, N. (2018), "Mechanism and remediation of water and sand inrush induced in an inclined shaft by large-tonnage vehicles", *Mine Water Environ.*, **37**(4), 849-855. https://doi.org/10.1007/s10230-018-0531-3.

Rafi, J.Y. and Stille, H. (2015), "Basic mechanism of elastic jacking and impact of fracture aperture change on grout spread, transmissivity and penetrability", *Tunn. Undergr. Sp. Technol.*, **49**, 174-187. https://doi.org/10.1016/j.tust.2015.04.002.

Sharma, K.M., Roy, D.G., Singh, P.K., Sharma, L.K. and Singh, T.N. (2017), "Parametric study of factors affecting fluid flow through a fracture", *Arab. J. Geosci.*, **10**(16), 362. https://doi.org/10.1007/s12517-017-3142-6.
Shi, L., Zhang, B., Wang, L., Wang, H.N. and Zhang, H.J. (2018), "Functional efficiency assessment of the water curtain system in an underground water-sealed oil storage cavern based on time-series monitoring data", *Eng. Geol.*, **239**, 79-95. https://doi.org/10.1016/j.enggeo.2018.03.015.
Stromsvik, H., Morud, J.C. and Grov, E. (2018), "Development of an algorithm to detect hydraulic jacking in high pressure rock mass grouting and introduction of the PF index", *Tunn. Undergr. Sp. Technol.*, **81**, 16-25. https://doi.org/10.1016/j.tust.2018.06.027.
Sui, W.H., Liu, J.Y., Hu, W., Qi, J.F. and Zhan, K.Y. (2015), "Experimental investigation on sealing efficiency of chemical grouting in rock fracture with flowing water", *Tunn. Undergr. Sp. Technol.*, **50**, 239-249. https://doi.org/10.1016/j.tust.2015.07.012.
Wanniarachchi, W.A.M., Ranjith, P.G., Perera, M.S.A., Rathnaweera, T.D., Zhang, C. and Zhang, D.C. (2018), "An integrated approach to simulate fracture permeability and flow characteristics using regenerated rock fracture from 3-D scanning: A numerical study", *J. Nat. Gas Sci. Eng.*, **53**, 249-262. https://doi.org/10.1016/j.jngse.2018.02.033.
Xiao, F., Zhao, Z.Y. and Chen, H.M. (2017), "A simplified model for predicting grout flow in fracture channels", *Tunn. Undergr. Sp. Technol.*, **70**, 11-18. https://doi.org/10.1016/j.tust.2017.06.024.
Xie, L.Z., Gao, C., Ren, L. and Li, C.B. (2015), "Numerical investigation of geometrical and hydraulic properties in a single rock fracture during shear displacement with the Navier-Stokes equations", *Environ. Earth Sci.*, **73**(11), 7061-7074. https://doi.org/10.1007/s12665-015-4256-3.
Yin, D.W., Chen, S.J., Chen, B., Liu, X.Q. and Ma, H.F. (2018), "Strength and failure characteristics of the rock-coal combined body with single joint in coal", *Geomech. Eng.*, **15**(3), 1113-1124. https://doi.org/10.12989/gae.2018.15.5.1113.
Zhang, Q.S., Zhang, L.Z., Liu, R.T., Li, S.C. and Zhang, Q.Q. (2017), "Grouting mechanism of quick setting slurry in rock fissure with consideration of viscosity variation with space", *Tunn. Undergr. Sp. Technol.*, **70**, 262-273. https://doi.org/10.1016/j.tust.2017.08.016.
Zhang, W. (2013), "The grouting diffusion model of power-law fluid in single fracture", *Appl. Mech. Mater.*, **477-478**, 524-530. https://doi.org/10.4028/www.scientific.net/AMM.477-478.524.
Zhao, Z.H. and Zhou, D. (2016), "Mechanical properties and failure modes of rock samples with grout-infilled flaws: A particle mechanics modeling", *J. Nat. Gas Sci. Eng.*, **34**, 702-715. https://doi.org/10.1016/j.jngse.2016.07.022.
Zuo, J.P., Li, Y.L., Liu, C.H., Liu, H.Y., Wang, J.T., Li, H.T. and Liu, L (2019), "Meso-fracture mechanism and its fracture toughness analysis of Longmaxi shale including different angles by means of M-SENB tests", *Eng. Fract. Mech.*, **215**, 178-192. https://doi.org/10.1016 /j.engfracmech.2019.05.009.

CC

List of symbols

JRC	Joint roughness coefficient
W/C	Water-cement ratio
τ	Shear stress
m	Power law coefficient
n	Power law index
ρ_f	Slurry density
u_f	Flow velocity
$\dot{\gamma}$	Shear rate
DV	Dimensionless value of pressure gradient
$\mathbf{J}_{i,j}$	Pressure gradient
i	Fracture width number
j	JRC number
b_e	Apparent fracture width
$\mathbf{\Gamma}_{\text{out}}$	Outlet boundary of model
$\mathbf{\Omega}$	Flow domain of model
α	Curve slope
NSD	No shear displacement
SD	Shear displacement
P	Pressure
Q	Flow volume
b	Fracture width
w_e	Width of slurry element
μ	Slurry viscosity
$\bar{\mu}$	Average slurry viscosity
v	Slurry velocity
$\bar{v}$	Average slurry velocity
b_h	Hydraulic fracture width
$\mathbf{\Gamma}_{\text{in}}$	Inlet boundary of model
$\mathbf{\Gamma}_{\text{w}}$	Wall boundary of model